Convective Heat Transfer Scaling of Ignition Delay and Burning Rate with Heat Flux and Stretch Rate in the Equivalent Low Stretch Apparatus

SANDRA OLSON
NASA Glenn Research Center at Lewis Field
21000 Brookpark Rd., mail stop 77-5
Cleveland, OH 44135 USA

ABSTRACT

To better evaluate the buoyant contributions to the convective cooling (or heating) inherent in normal-gravity material flammability test methods, we derive a convective heat transfer correlation that can be used to account for the forced convective stretch effects on the net radiant heat flux for both ignition delay time and burning rate. The Equivalent Low Stretch Apparatus (ELSA) uses an inverted cone heater to minimize buoyant effects while at the same time providing a forced stagnation flow on the sample, which ignites and burns as a ceiling fire. Ignition delay and burning rate data is correlated with incident heat flux and convective heat transfer and compared to results from other test methods and fuel geometries using similarity to determine the equivalent stretch rates and thus convective cooling (or heating) rates for those geometries. With this correlation methodology, buoyant effects inherent in normal gravity material flammability test methods can be estimated, to better apply the test results to low stretch environments relevant to spacecraft material selection.

KEYWORDS: radiant cone heater, ignition delay, burning rate, convective heat transfer, low stretch

INTRODUCTION

The Equivalent Low Stretch Apparatus (ELSA), shown in Figure 1, uses an inverted cone geometry with the sample ignition and burning in a ceiling fire (stagnation flow) configuration. In this configuration, the influence of buoyancy is reduced because the rise of hot gases is inhibited. The buoyant stagnation flow around the sample acts in the same direction as a variable forced convective stagnation flow, so that the mixed convective stretch rate (velocity gradient) near the fuel surface can be varied [1-3].
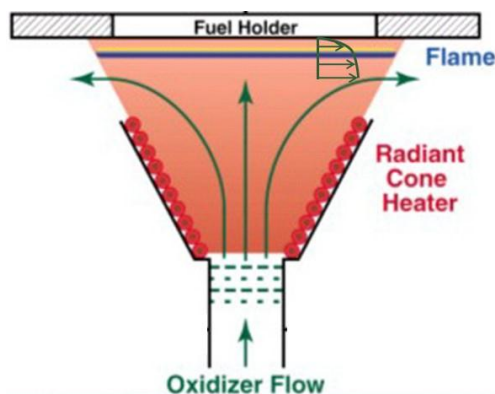

Figure 1: A schematic of the Equivalent Low Stretch Apparatus (ELSA), showing the stagnation boundary layer that develops on the sample.

Equivalent stretch rates can be determined as a function of gravity, imposed flow, and geometry. A generalized expression for stretch rate which captures mixed convection includes both buoyant and forced stretch is defined [1] as $a_{equivalent} = a_f(1 + a_b^2/a_f^2)^{1/2}$. The forced flow stretch rate is characterized by $a_f = U_{jet}/d_{jet}$ for a jet impinging on a planar surface [4], where U_{jet} is the velocity the jet and d_{jet} is the

diameter of the jet. The buoyant stagnation flow is ~4 s^{-1} [4], and scales with gravity as $a_b \sim [g/R]^{\frac{1}{2}}$ [1,2], where g is gravity and R is the radius of curvature of the sample.

The 10 cm square sample is ignited and burned above the radiant heater. In this configuration, the velocity gradient normal to the flame sheet is dominated by the velocity of the incoming flow rather than buoyancy except at very low jet velocities. Tests have been performed on various materials such as Combitherm™, Kevlar™, Nomex™, Pyrell™ foam, and Kydex™ to evaluate the suitability of this test for a range of materials. Modeling of the flow field, and flow visualization in the hardware have demonstrated very low stretch rates (~4 s^{-1}) [5]. Figure 2 shows an isothermal flow visualization image at 5 s^{-1} as well as an FDS model [6] W-velocity gradient for a 30 cm/s jet and a 7.5 cm diameter nozzle with the cone at 950 K and the sample at 600 K. The inset to Fig. 2b shows the centerline gradient evaluated from 3 cm <Z<9 cm compared to U/d stretch scaling. The computed gradient agrees with stretch rate predicted by theory.
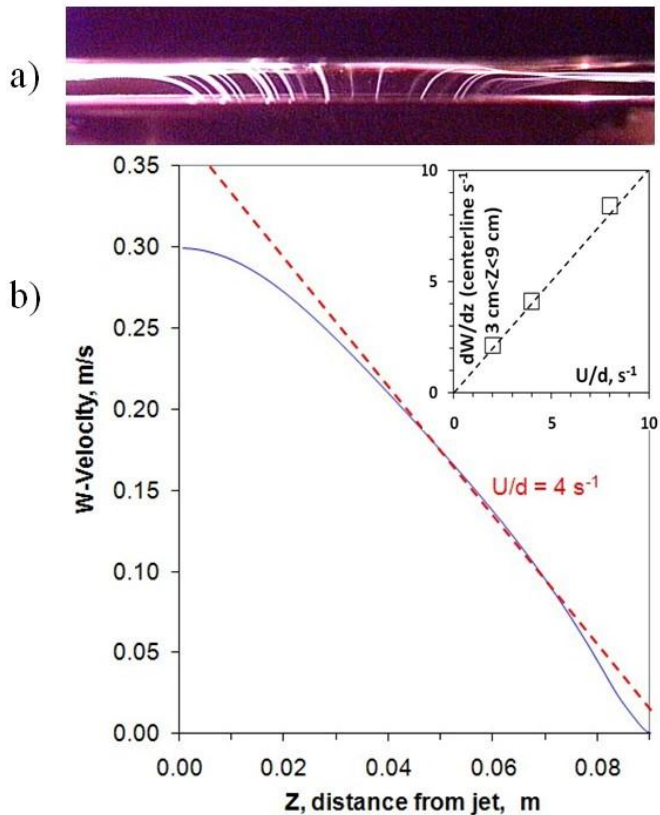

Figure 2: a) Flow visualization in inverted cone geometry showing stagnation flow impinging on the sample after exiting the cone. b) FDS computation of cone geometry W-velocity profile for a case with theoretical stretch rate of 4 s-1 with a hot cone (950K) and hot sample (600 K). Inset shows FDS velocity gradient dW/dZ, evaluated from 3<Z<9, compared to U/d stretch scaling.

BOUNDARY LAYER SCALING

Wichman [7] proposed that the flame spreading mechanism is controlled by local conditions of the flow field, as described by the surface velocity gradient. This implies that the flame spread rates measured in two (or more) different experiments may be identical even though the external flow conditions of these experiments differ significantly (for all other factors such as free-stream oxidizer concentration and solid fuel material remaining the same).

Blasius boundary layer theory provides a linear velocity profile near the wall, which is a constant stretch (velocity gradient) environment. Notice in Figure 3 that in the boundary layer region $0 \leq \eta \leq 1$; $0 \leq U/U_\infty \leq 0.63$ the gradient is linear. Flames that reside within this region are subject to a constant stretch rate. For forced flow velocities of 0-20 cm/s (near-wall spacecraft ventilation flows), the velocity gradient (stretch rate) is 0-33 s^{-1} for small fires (x=5 cm), as shown in the inset to Figure 3. The stagnation boundary layer, shown schematically in Figure 1, can thus be related to other flow geometries.
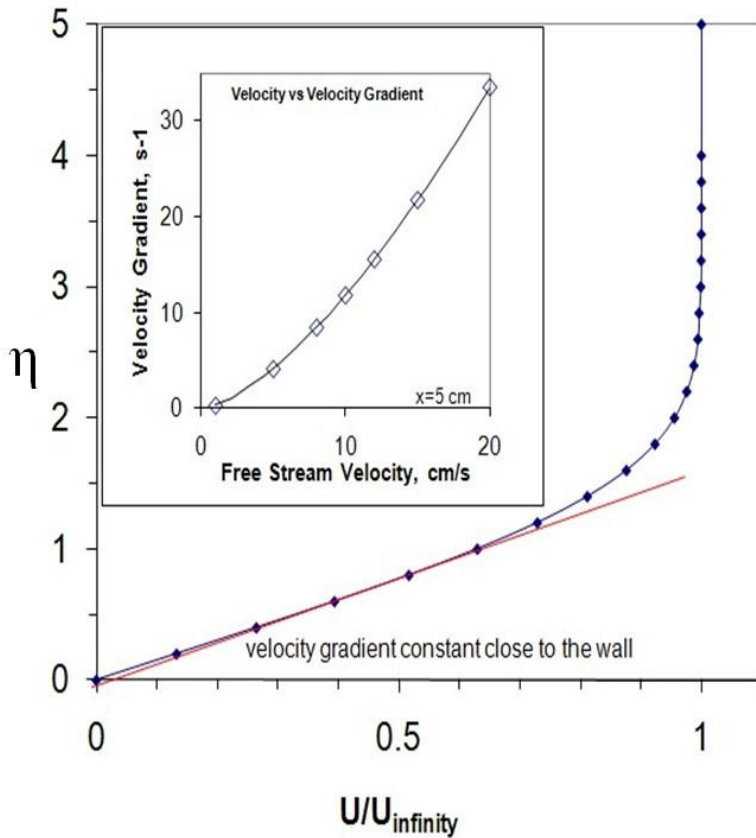

Figure 3: Linear velocity profile showing constant velocity gradient ('stretch rate') within boundary layer. Velocity gradient as a function of free stream velocity is shown in the inset.

To demonstrate this scaling concept with experimental results, the ignition delay time results of FIST (Forced Ignition and flame Spread Test) experiments during low gravity parabolic aircraft testing [8] at different flow rates, including natural convection, are added to the previous ignition delay time data [4] in a new ignition delay-stretch rate or equivalent gravity level plot, shown in Figure 4, by estimating the Blasius boundary layer velocity gradient at the surface for the free stream flow based on the FIST experiment geometry (gradient evaluated at x=22 cm) . The stretch correlation holds up very well up to ~ 100 s^{-1} stretch rates, but breaks down at very high forced flow stretch rates (not shown), possibly due to a transition to turbulent flow affecting the entrance length boundary layer flow within the duct, and thus affecting the convective heat and mass transfer.

Also included is the 1g standard cone data, with a secondary equivalent gravity level axis shown below the equivalent stretch rate axis based on Froude number scaling (Fr=U/(gd)$^{1/2}$). For a=U/d, a constant Froude number and geometry provides $a \sim g^{1/2}$, in agreement with the above $a_b \sim [g/R]^{1/2}$ [1,2] Using the buoyancy-dominated normal cone result that indicates that 1g ~ 33 s^{-1} [4] and this scaling allows the calculation of this second axis in both Figure 4 and Figure 5. ELSA data is in the partial gravity range.
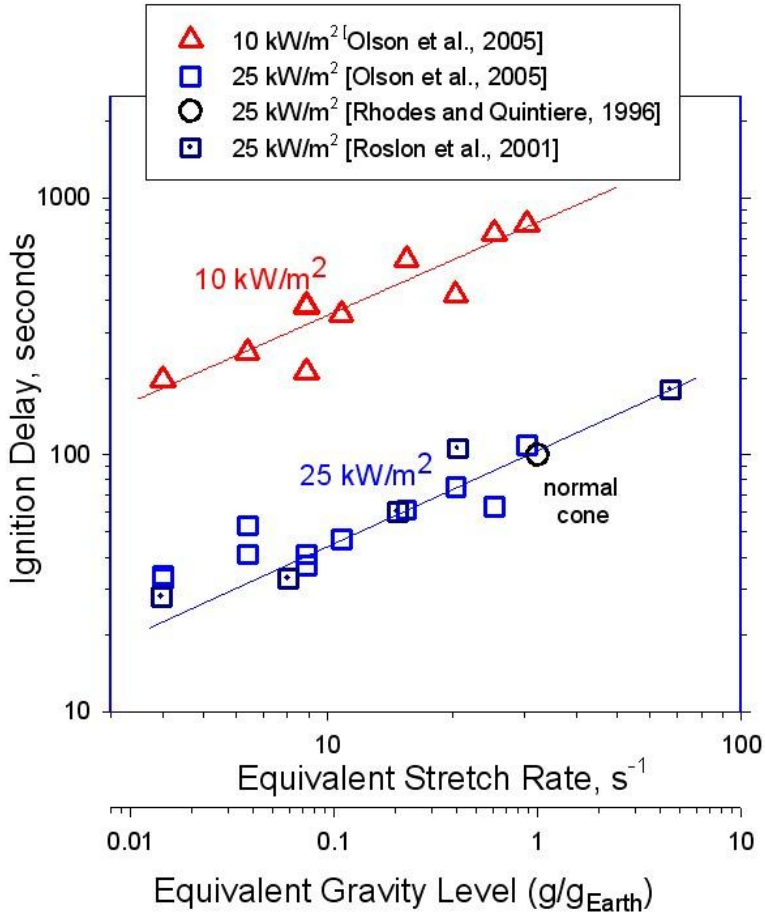
Figure 4: Using boundary layer velocity gradient scaling, FIST KC-135 (Roslon et al.) [8] and 1g cone (Rhodes and Quintiere) [9] ignition delay time data is plotted with previous data [4], and shows good trend agreement.

REGRESSION RATE

Stretch is induced not only by velocity gradients, but also by flame curvature. A flammability study of different materials, including PMMA, was conducted aboard Mir in their Skorost facility [10,11]. Rods of PMMA were burned in a concurrent airflow parallel to the rod axis. Interestingly, the rods developed large molten balls at their burning tips, and in the low flow environment provided by Skorost, the flames were stabilized at the stagnation point of the ball. They measured rod regression rates, molten ball diameters, and flame diameters as a function of ambient forced flow. Using that information, we can estimate the stretch rates and burning rates for these PMMA balls.

Regression rates of molten spheres were calculated by converting the mass loss rate (g/s) determined from the reported average rod regression rate into the same mass loss rate from the reported size of the molten sphere. The inviscid forced stretch around the sphere is given by $a_{f,sphere} = 3/2\ U/R_{sphere}$, and the curvature-induced stretch is estimated for the small samples from $a_{curv} = [3\ U/R_{sphere}]\ *[(R_{flame}-R_{sphere})/R_{sphere}]$. The equivalent stretch in this case is approximated as $a_{equiv} = a_{f,sphere} + a_{curv}$. As the flame standoff distance ($R_{flame}-R_{sphere}$) becomes small relative to the radius of curvature, curvature effects become negligible. However, for the small spheres in these experiments (<1cm), the curvature effects were significant and needed to be accounted for. The data is plotted in Figure 5.
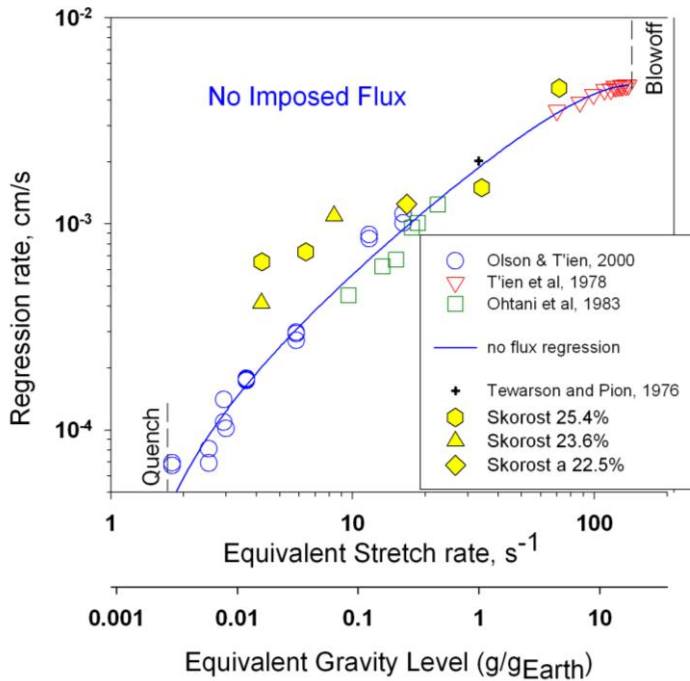
Figure 5: Graph comparing low stretch flame results [2] with Skorost tests conducted aboard Mir [10, 11], and 1g data [12]. While the oxygen concentrations aboard Mir were elevated (other data was obtained in air), the agreement is generally good.

The comparison between Skorost results [10, 11] and low stretch average regression rate PMMA results [2,13,14] is very good, especially considering the Skorost tests were conducted in slightly higher oxygen concentrations, which explains why the data is biased above the curve and deviates more at lower stretch where diffusive oxygen transport is more significant. The flame heat release rate will be affected by the ambient oxygen concentration, and an increase in oxygen will result in an increase in the flame heat flux back to the fuel surface, resulting in an increase in burning rate. Lastly, notice on the secondary axis that the data is for conditions corresponding to the partial gravity levels and stretch rates associated with spacecraft ventilation.

IGNITION DELAY

At low gravity, radiation from a small adjacent burning material may be sufficient to ignite a material. This was observed on Mir [10, 11] in their Skorost facility, where the burning molten ball of fuel at the end of a rod of one material heated an adjacent rod to vaporization temperatures (bending, bubbling). The flame from the first rod then acted as the gas-phase pilot for the premixed cloud that developed between the two rods. The premixed flame propagated through the cloud and ignited the heated second rod. The critical heat flux for ignition in the absence of convective cooling is just slightly more than offsets the experimental heat losses such as surface radiation at T_{ign} [4], which agrees with the model of Rhodes and Quintiere [9] in the limit of no convection, and is consistent with observations that ignition is easier in microgravity [15].

For thermally-thick fuels, the heat-up time is the dominant timescale that controls the ignition delay time. The ignition delay time of a thermally thick fuel exposed to an incident radiative heat flux can be expressed as [16]:

$$\frac{1}{\sqrt{t_{ign}}} = \frac{2}{\sqrt{\pi}} \frac{1}{\sqrt{k\rho c}} \frac{\dot{q}''_{net}}{(T_{ign} - T_{\infty})} \qquad (1)$$

Inverse square root of ignition delay time versus heat flux graphs thus have a linear trend, and the slope of the line is related to the fuel properties ($k\rho c$) and (T_{ign}-T_{∞}). However, the slope of the line has been found to be apparatus-dependent, and not derivable from fundamental fuel properties [17-19]

Ignition delay time is defined as the time between when the sample is exposed to the radiant heater and the time at which sustained ignition is achieved. Ignition delay has been measured as a function of stretch rate for thick PMMA samples at 10 kW/m^2 and 25 kW/m^2 flux levels [4], as shown in Figure 4. For a fixed radiant flux, ignition delay times are shown to decrease with decreasing equivalent velocity gradient, or g level.

At 25 kW/m^2 the difference between a normal (1-g) cone ignition delay time (high equivalent velocity gradient) and ignition delay times at very low equivalent velocity gradients is a factor of three (see Figure 4), demonstrating that ignition delay times determined from normal cone tests significantly overestimate the ignition delay times of materials in microgravity or in partial gravity extraterrestrial environments. In addition, at the 10 kW/m^2 flux level, the ignition delay time at low g levels approaches the value of the 1-g normal cone at 25 kW/m^2, indicating the sensitivity of low g flames to even weak levels of external flux.

The difference between ignition delay times in a normal-gravity cone and ELSA is also shown in Figure 6 for Kydex 100, a PMMA-PVC blend material commonly used for aircraft interior cabin walls. Kydex 100 sheets (0.15 cm thick) were ignited in ELSA under no forced stretch rate (a_b~4 s^{-1}). Ignition delay time is consistently shorter in ELSA, indicating faster ignition times with reduced convective cooling. The slopes of the curve fits fall between thermally-thick (slope ~ -2) and thermally-thin (slope ~ -1), indicating this fuel is of intermediate thickness.

It is interesting to note that Kydex 100 passes NASA STD-6001 Test 1 (upward flammability test) at both 14.7 psia, 20.9% O_2 and at 14.3 psia, 25.9% O_2 [20]. However, it only requires a modest 15 kW/m^2 of external heat flux to ignite the material in air in NASA STD-6001 Test 2 (cone calorimeter test) [20].
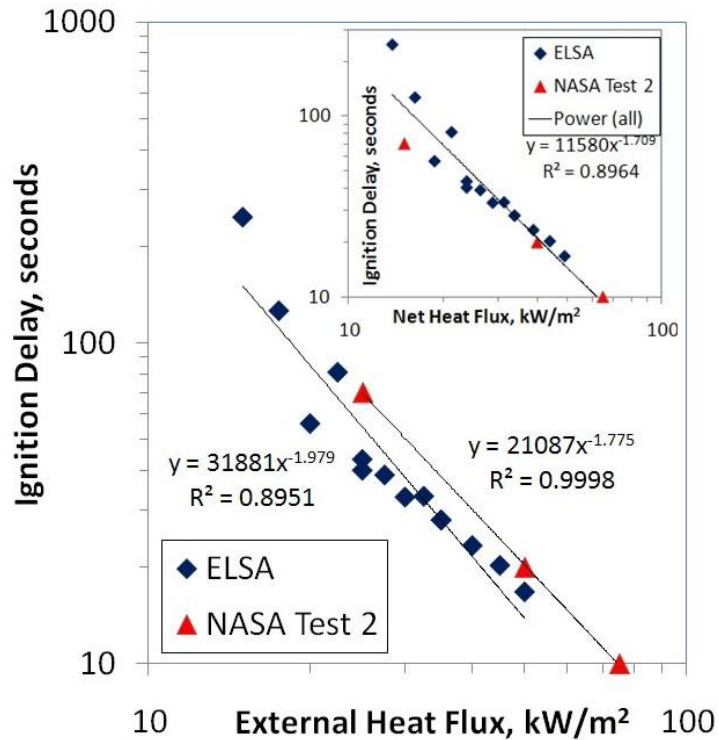

Figure 6: New ignition delay time data for Kydex 100 versus external heat flux for ELSA is compared to ignition delay obtained in a standard cone calorimeter in 1g [20]. Standard cone data consistently takes longer to ignite for the same external heat flux due to convective cooling. Inset shows when cooling is accounted for using the convective cooling correlation discussed below, ignition delay data agrees much better.

CONVECTIVE HEAT TRANSFER CORRELATIONS

One of the major difficulties in evaluating a material's flammability is that different tests rank materials differently. Standard material flammability test methods each provide a unique flow environment with its associated convective heat transfer, and thus direct comparisons between test methods is difficult [17]. Most fires are diffusion flames which reside within a fluid mechanical boundary layer, with a bulk flow either due to forced convection or driven by buoyancy. The flow can be parallel to the fuel, or orthogonal to it, or a combination of the two. For example, the LIFT (Lateral Ignition Flame spread Test) apparatus provides a natural convective boundary layer on the vertical sample, whereas the FPA (Fire Propagation Apparatus) provides an upward coaxial forced flow past the horizontal sample. The cone calorimeter has natural convection across the horizontal (or vertical) sample, and ELSA provides a stagnation flow impinging on the sample.

Unfortunately, ignition delay time data from different radiant ignition test methods have different slopes, resulting in different TRP values [18]. For example, the $k\rho c$ values reported for PMMA using the LIFT methodology over-predict by a factor of more than four the product of the individual property values [19]. The property values derived from Eq. 1 have been found to be dependent on flow conditions.

The primary reason different tests do not provide the same slope is because of the different convective environments of the tests. To better evaluate the buoyant contributions to the convective cooling (or heating) inherent in normal-gravity test methods, we derive a convective heat transfer correlation that can be used to account for the forced convective stretch effects on the net radiant heat flux for both ignition delay time and burning rate.

For a thermally-thick fuel, the heat-up time is much longer than the gas-phase mixing time. Thus, the ignition delay is driven by the net heat flux. As the net heat flux increases (via reduced convective cooling, for example), the inverse square root of the ignition delay time increases (ignition delay time decreases). From Fernandez-Pello [21], the net flux for stagnation flow can be estimated as $q''_{net} = q''_{external} + q''_c - q''_{rad}$, which corrects for convective and surface radiation.

During heat-up, the convective heat transfer increases as the temperature difference between the ambient air flow and the heating surface increases. The convective heat cooling rate is thus a maximum at ignition. After ignition, the presence of the flame and the buoyant flow result in a convective heating effect. The fluid dynamics and heat transfer associated with impinging jets is very complex, and still not completely understood, and there is no generally established functional relationship with Nussult number [22]. The convective heat transfer coefficient can be related to stretch rate through similarity between thermal and viscous boundary layers. It is reasonable to approximate that the convective heat transfer coefficient h_c is proportional to a, the stretch rate. This linear approximation has a better empirical fit to the data than the classic square root dependence, where data at different stretch rates remain stratified.

Prior to ignition, forced convection of ambient air to the irradiated hot surface has a cooling effect, whereas after ignition, an increase in the stagnation flow presses the flame closer to the fuel surface, increasing the heat flux. We estimate the convective effect to be $q''_c = (0.001*a)*\Delta T$ kW/m^2, where ΔT is ~ -300 K for ignition and ~ 1000 K for burning. For the range of stretch rates of interest (2-200 s^{-1}, Figure 5 x-axis), the heat transfer coefficient ($h_c = (0.001*a)$) varies over a reasonable range of 0.002-0.2 kW/m^{2}K. This convective heat transfer estimate is used in Eq. 1 to correlate the data for both ignition delay and also to correlate the regression rate.

For ignition, Eq. 1 without the radiant loss term becomes

$$\frac{1}{\sqrt{t_{ign}}} = \frac{2}{\sqrt{\pi}} \frac{1}{\sqrt{k\rho c}} \left[\frac{\alpha q''_{ext} - 0.3a}{(T_{ign} - T_\infty)} \right] \qquad (2)$$

where the $q''_c = (0.001*a)*-300K = -0.3a$ kW/m^2 is the convective heat transfer estimate from above for ignition and α is absorptivity, assumed to be equal to one. Radiant heat loss (q''_{rad}) is neglected since it is approximately 5 kW/m^2 and will simply shift all of the results uniformly for the assumed constant T_{ign}.

We use this relationship as a guide to correlate the thermally-thick PMMA ignition delay time with net heat flux in Figure 7. Stretch rates vary from the buoyant limit of 4 s^{-1} [4] to 33 s^{-1}, and imposed heat flux varies from 10-75 kW/m^2. The data fits well using the correlation, despite the differences in the experiments. Normal gravity high velocity FIST data (m/s flow rates, not shown), however, does not – probably due to turbulence. Low heat flux high convective cooling data shows more scatter, which may be due to an overestimation of convective cooling or variation in ignition temperature (Eq. 2) for these near limit very slow ignition tests.

The power law fit has a weaker dependence on net flux than predicted by Eq. 2. Rather than an exponent of -2, the best fit power law exponent is only -1.43, which is even lower than the Kydex data from Figure 6. It is likely that the thermal theory assumption of a constant ignition temperature does not hold throughout the ignitable range.

In Figure 7, a second equivalent gravity axis is again shown, using the same stretch scaling discussed above, along with normal cone ignition delay-heat flux data [23]. To fix the g axis, a net heat flux of 15.1 kW/m2 at 1g was used (25 kW/m2 – 0.3*33 s^{-1}, [9]). This axis is only a scaling approximation to demonstrate that as gravity decreases, ignition delays become shorter as convective cooling decreases.
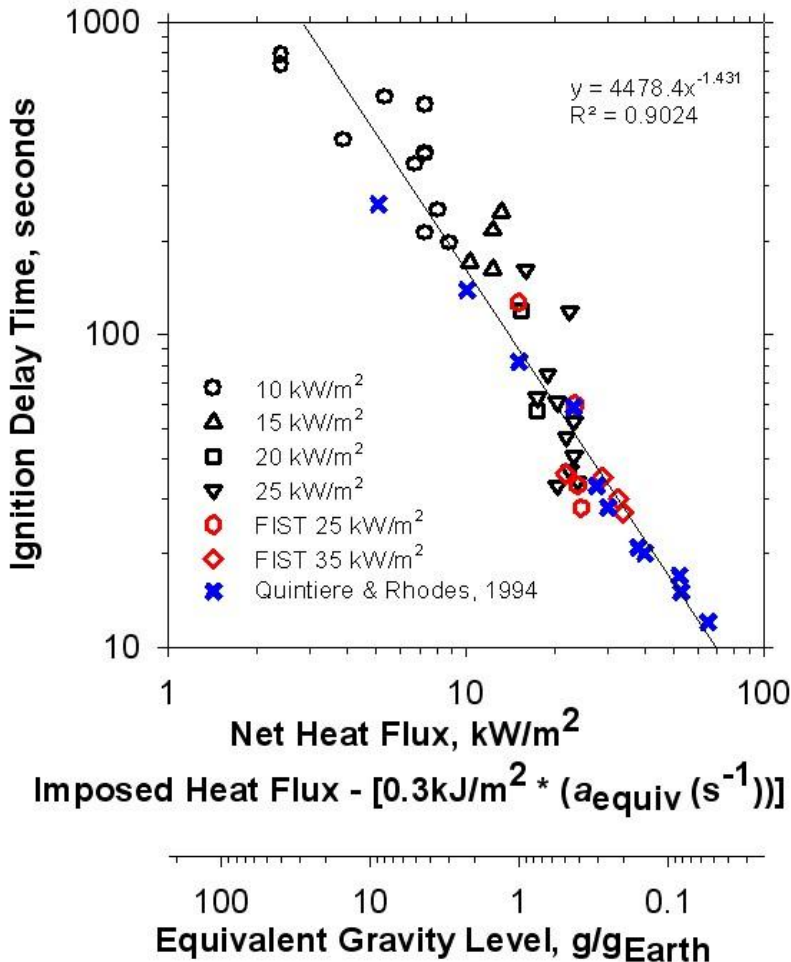

Figure 7: Ignition delay time for PMMA correlated with net heat flux which includes convective cooling effects. ELSA (clear PMMA) [4], normal cone (black PMMA) [23] and low gravity FIST data (clear PMMA) [8] agree well.

Regression data can be evaluated in the same light. For steady burning, using the above estimate and 1000 K for the difference between flame temperature and burning surface temperature, the convective heating effect is $q''_c = +1a$ kW/m^2, where the empirical convective coefficient for burning is 1 kJ/m^2. The effect of increasing stretch in the stagnation flow geometry is to push the flame closer to the fuel, in effect increasing the heat flux from the flame to the surface. Using this correlation, the 1g normal cone equivalent stretch rate of 33 s^{-1} [4] results in a flame heat flux of 33 kW/m^2, which is in good agreement with the measured flame heat flux of 37 kW/m^2 [23] and estimated heat flux of 38.5 kW/m2 [12].

As shown in Figure 8, which is a revised version of the no external heat flux data shown in Figure 5 that now also includes external heat flux data [4], this correlation holds up very well over a 0-25 kW/m^2 range of external flux and stretch rates from 2-150 s^{-1}. The Skorost data [10, 11] again trends high especially at low stretch due to the elevated oxygen concentrations on Mir while the rest of the data was taken in ambient air. At higher oxygen, flame heat release rate will be higher, resulting in a higher heat flux than air, so the data would shift to the right if the difference oxygen were accounted for. Estimates of that correction do shift the very low velocity tests correctly, but the higher flow tests (up to 8 cm/s) are shifted too much by the correction, possibly due to a transition to an excess air (fuel lean) condition in the assumed relevant flow volume. The regression rate (or burning rate if regression rate is divided by the fuel density) is linearly proportional to the net heat flux over most of the flammable range, and only falls off this linearity near blowoff and quenching extinction.

Also in Figure 8, a second equivalent gravity axis is again shown, using the same stretch scaling discussed above, along with normal cone regression rate-heat flux data (25 kW/m^2+(1*33 s^{-1}=)[9, 12]. This axis is only a scaling approximation to demonstrate that as gravity increases, regression rate increases since the flame is pressed closer to the fuel at higher g levels, increasing the burning rate.
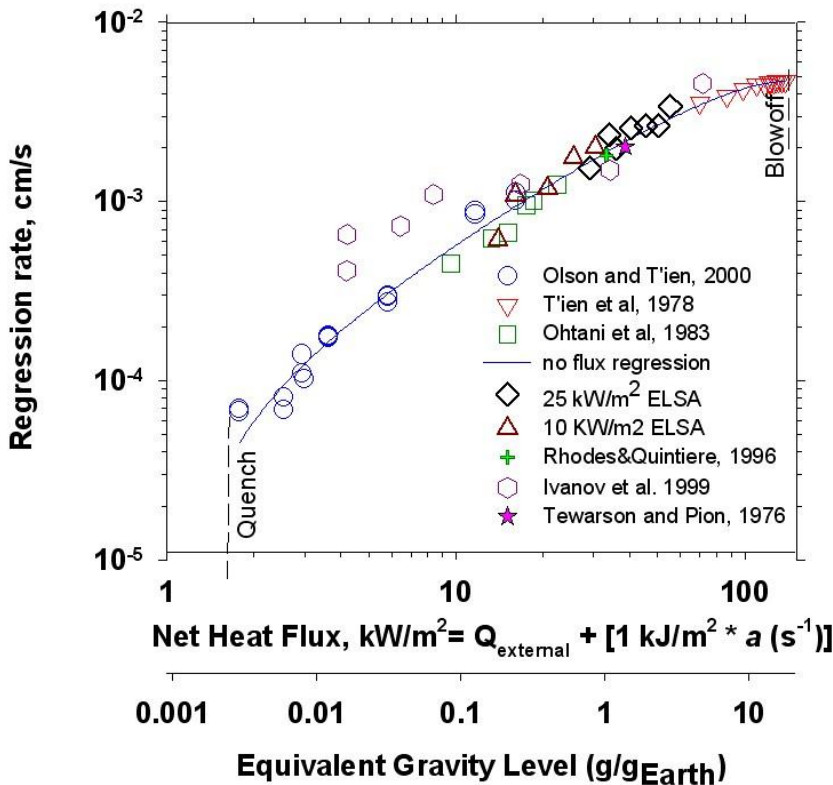

Figure 8: PMMA regression rate data [2, 13, 14, 4, 9, 10, 11, 12] correlated with net flux. Data from references as noted in legend. Some data with external heat flux and stretch rate, other data no external heat flux. No external heat flux data from [12] is estimated flame to surface heat flux (Table 3) and "ideal" burning rate data for PMMA (Table 4).

CONCLUDING REMARKS

ELSA ignition delay and burning rate data can be compared with data in other geometries and gravity levels using flow similarity. Correlations of combined radiative and convective heat transfer effects on the ignition delay (cooling effect) and burning rate (heating effect) are provided that collapse the data from disparate test environments. When convective heat transfer is accounted for in the net heat flux to the solid, normal gravity material flammability test methods for ignition delay or burning rate can be applied to low gravity environments.

ACKNOWLEDGMENTS

REFERENCES

[1] D.W. Foutch, J.S. T'ien, "Extinction of a Stagnation-Point Diffusion Flame at Reduced Gravity", AIAA J. 25 (7) (1987) 972-976.

[2] S.L. Olson, J.S. T'ien, "Buoyant Low Stretch Diffusion Flames Beneath Cylindrical PMMA Samples", Combust. Flame.121 (2000) 439-452.

[3] J.B. Armstrong, S.L. Olson, J.S. T'ien, "Transient Model and Experimental Validation of Low Stretch Solid-Fuel Flame Extinction and Stabilization in Response to a Step Change in Gravity", Combust. Flame 147 (2006) 262-277.

[4] S.L. Olson, H.D. Beeson, J.P. Haas, J.S. Baas, "An Earth-Based Equivalent Low Stretch Apparatus for Material Flammability Assessment in Microgravity and Extraterrestrial Environments", Proc. Combust. Inst. 30(2) (2005) 2335-2343.

[5] F.J. Miller, S.L. Olson, S.A. Gokoglu, P.V. Ferkul, "Material Flammability Test Methods for Achieving Simulated Low-Gravity Conditions", 5th US Combustion Meeting, The Combustion Institute, San Diego, CA, March 25-28, 2007.

[6] K. McGrattan, S. Hostikka, J. Floyd, "Fire Dynamics Simulator User's Guide", NIST Special Publication 1019-5, 2009. Also http://fire.nist.gov/fds/

[7] I.S. Wichman, "Flame Spread in an Opposed Flow with a Linear Velocity Gradient", Combust .Flame 50, (1983) 287-304.

[8] M. Roslon, S. Olenick, Y.Y. Zhou, D.C. Walther, J.L. Torero, A.C. Fernandez-Pello, H.D. Ross, "Microgravity Ignition Delay of Solid Fuels in Low Velocity Flows", AIAA J. 39 (12) (2001) 2336-2342.

[9] B.T. Rhodes, J.G. Quintiere, Fire Safety J. 26, (1996) 221-240.

[10] A.V. Ivanov, Ye.V. Balashov, T.V. Andreeva, A.S. Melikhov, "Experimental Verification of Material Flammability in Space", NASA CR-1999-209405, 1999.

[11] A.V. Ivanov, V.F. Alymov, A.B. Smirnov, S.P. Shalayev, D.Ye. Belov, Ye. V. Balashov, T.V. Andreeva, A.V. Semenov, A.S. Melikhov, I.A. Bolodyan, V. I. Potyakin, "Preliminary Results of the Third Test Series of Nonmetal Material Flammability Evaluation in SKOROST Apparatus on the Space Station Mir, NASA CP-1999-208917, 47-50.

[12] A. Tewarson, R.F. Pion, Combust.Flame 26 (1976) 85-103.

[13] J.S.T'ien, S.N. Singhal, D.P. Harrold, J.M. Prahl, Combust. Flame 33 (1978) 55–68.

[14] Ohtani, K. Akita, T. Hirano, Combust. Flame 53 (1983) 33–40.

[15] S.L. Olson, T. Kashiwagi, O. Fujita, M. Kikuchi, K. Ito, "Experimental Observations of Spot Radiative Ignition and Subsequent Three-Dimensional Flame Spread over Thin Cellulose Fuels", Combust. Flame 125 (2001) 852-864.

[16] A. Tewarson, Generation of heat and chemical compounds in fires. The SFPE Handbook of Fire Protection Engineering (3rd Edition). Section 3, Chapter 4. The National Fire protection Association Press: Quincy, MA, 2002; 3–161.

[17]   M.A. Dietenberger, "Ignitability Analysis Using the Cone Calorimeter and Lift Apparatus", Proc. Intl. Conf. Fire Safety 22 (1996)189-197.

[18]   J.G. Quintiere, "A theoretical basis for flammability properties", Fire and Materials 30, (2005) 175-214.

[19]   F.W. Mowrer, "An Analysis of Effective Thermal Properties of Thermally Thick Materials", NIST GCR 03-855, 2003.

[20]   D. Mulville, "Flammability, odor, offgassing, and compatibility requirements and test procedures for materials in environments that support combustion", NASA-STD-6001, 1998.

[21]   A.C. Fernandez-Pello, The Solid Phase, Chapter 2 in   G. Cox (Ed.), Combustion Fundamentals of Fire, Academic Press, 1995.

[22]   Meola, C., "A New Correlation of Nusselt Number for Impinging Jets", Heat Transfer Engineering 30(3): 221-228, 2009.

[23]   Quintiere, J.G., and Rhodes, B.; "Fire Growth Models for Materials", NIST-GCR-94-647, 1994.